Indentation of bituminous coals: Fracture, crushing and dust formation

By Elena L. Kossovich[a], Feodor M. Borodich[b], Svetlana A. Epshtein[a], Boris A. Galanov[c]

[a] *Laboratory of Physics and Chemistry of Coals, Mining Institute, National University of Science and Technology "MISiS", 119049 Moscow, Russia*
[b] *School of Engineering, Cardiff University, Cardiff CF24 0AA, UK*
[c] *Institute for Problems in Materials Science, National Academy of Sciences of Ukraine, 3 Krzhyzhanovsky St., Kiev 03142, Ukraine*

Abstract

Bituminous coals are still the main source of energy in the world. However, these brittle porous materials are prone to crushing under action of industrial tools. Our early depth-sensing nanoindentation tests of bituminous coals showed that even if the depth of indentation is within the nanoscale, these brittle coals are no longer continuous elastic media within the indentation zone but rather fine powders of crushed particles irrespectively to the coal maceral. Dust formation of the materials is a problem of great practical importance for the mining industry. Indeed, the powders of coal particles formed during crushing may cause not only explosions in mines but they also contaminate the environment around the roads of the coal transportation. In this study, the crushing of coals due to action of rigid conical indenters and formation of small coal particles is investigated. The studies are based on development of the Galanov-Grigoriev (GG) model of crushing of brittle porous materials and the model adjustment to specific features of coal fracture. Using the indentation tests, we estimate the size distribution of the dust particles formed within the region of fully crushed material. Results are presented for coals of three different stages of metamorphism.

Keywords: indentation; Galanov-Grigoriev model; dust formation; porous brittle media; coals

1 Introduction

The term 'coal' does not mean a specific material having well known material properties. One can say that coal is a naturally sedimentary rock having an organic genesis. Actually, coals are sedimentary materials composed of a number of distinct organic entities called macerals and some amount of inorganic substances along with internal pores and cracks. They contain also water and gases in submicroscopic pores (Neavel 1981, Xie 2015). Hence, the term includes a wide class of materials having extremely complex heterogeneous internal structure. The coals are usually classified as peat, brown coals (also known as "lignites"), bituminous coals (also known as "steam coal", "rock coals", and "hard coals") and anthracite. High pressure, relatively high temperatures, and time metamorphose low-rank coals into bituminous coals and anthracite. The degree of metamorphism is an important feature of coal that reflects changes in coal components, structures, and properties. The maceral composition of coals is

defined by many factors such as specific features of the coalification processes, the nature of the initial plant material and the conditions of its accumulation and decomposition (Epshtein et al. 2015). The carbon contain of coals varies from 65 to 95 % depending on the degree of the coal metamorphism. Here we concentrate on bituminous coals that are the most important and the most widely spread kind of coals (Xie 2015).

Formation of coal dust particles is a problem of great practical importance for mining industry. The coal dust may cause explosions in mines. The problem of coal dust formation is also important for environmental studies. As it was noted by Kossovich et al. (2019b), the coal dust is a significant threat to the safety of people and to the environment because the fine coal dust particles whose sizes are less than 25 μm are able to stay in the air for a long period of time. These particles may also appear during mining, storage, transportation and processing of coals. The coal dust may contaminate the environment around the roads of the coal transportation. Our studies are based on modelling of indentation tests in porous materials and development of the Galanov-Grigoriev (GG) model of crushing of brittle porous materials (Galanov and Grigoriev 2006).

Indentation techniques are traditionally used for determination of some mechanical characteristics of materials (Grigorovich 1976, Fischer-Cripps 2011). In particular, many papers of geomechanics and civil engineering are devoted to studies of mechanical properties of rocks and cement pastes by indentation techniques (see, e.g. reviews by Meyers 1982 and Constantinides et al. 2003). Microindentation tests are also very popular in application to coals (see, e.g. Musyal 1963, GOST 21206-75, Epshtein et al. 2007, Hower et al. 2008, Kožušníková 2009). For example, the state standard (GOST 21206-75) applies to coal and anthracite and establishes methods for determining the microhardness and microbrittleness of vitrinite of coal and anthracite in polished briquettes and polished pieces. The standard was introduced in Soviet Union and it is still valid in Russia, Ukraine, and many other countries of the former Soviet Union.

The depth-sensing nanoindentation (DSNI) techniques enabled us to examine mechanical properties of coal organic components belonging to different groups of macerals using a new procedure based on the joint application of continuous nanoindentation and optical microscopy (Borodich et al. 2015, Epshtein et al. 2015). Later these techniques were developed further and discussed in several papers (Kossovich et al. 2016, 2019a, Argatov et al. 2017). Nowadays the DSNI tests of coal samples are used worldwide (see, e.g. Vranjes et al. 2018). However, the traditional indentation techniques at both micro and nano scales usually do not consider fractures of materials.

On the other hand, problems of contact between a rigid indenter and a brittle material resulting in cracking were studied by many authors. Hertz was the first researcher who mentioned creation of cracks due to punch indentation; then the problems related to crack formation during indentation into brittle and elastic-plastic materials were intensively studied, see, e.g. a literature review by Lawn (1993) and Kolesnikov and Morozov (1989). A rather sophisticated behaviour is observed in glass samples under action of a small spherical indenter: median cracks and plastic deformation within a core region along with occasionally Hertzian cone cracks form during the loading cycle, while radial cracks and lateral cracks occur on the unloading cycle (Lawn 1993, Kolesnikov and Morozov, 1989). The microbrittleness of minerals and coals is usually calculated using the idea introduced by Bernhardt (1941). He argued, that if the load during microindentation of a brittle material is below some critical

load P_{cr} specific for the material, then one does not observe cracking. This observation was employed for estimation of the microbrittleness of minerals and coals. Usually the number of imprints producing cracks in a group of 100 imprints of a sample is calculated and this number is used as the microbrittleness characteristics (Musyal 1963, Epshtein *et al.* 2007). However, destruction of many natural and artificial materials may result not only in creation of a crack or system of cracks but also in crushing of materials. Indeed, depth-sensing nanoindentation tests of thin coal sections glues to a a hard substrate (see Borodich et al. (2015) for further detail of tests) revealed a significant influence of the glue layer on the obtained experimental data. The values of effective modulus of coal macerals glued to the substrate estimated by the usual procedure introduced by Oliver and Pharr (1992) depend strongly on the maximum depth of indentation. Fitting of the experimental data by several popular approximating functions, showed that many of these functions do not reflect the data trends for both vitrinite and inertinite macerals (Kossovich et al. 2016). These surprising observations were explained by Argatov et al. (2017) employing asymptotic models. It was shown that the above mentioned popular approximating functions can be successfully used for metallic samples whose internal structure is not changed by nanindenters. However, even if the indentation depth is within the nanoscale, these brittle coals are no longer continuous elastic media within the indentation zone but rather fine powders of crushed particles irrespectively of the coal maceral (Argatov et al. 2017). This paper is devoted mainly to theoretical modelling of crushing of coals under action of an indenter and to questions related to the estimations of coal dust particle distributions. However, the results may be also applied to other porous materials.

2 Indentation of porous brittle materials and coals.

We believe that modelling of porous materials is somehow similar to modelling of steel samples. Indeed, at the micro/nano scales steels consist of collections of anisotropic crystals, however if one considers fracture at meso or macroscales then steel samples are modelled as isotropic homogeneous solids. We assume that the same approach is valid in application to coals. At micro/nano scales they consist of different components, however, to model fracture of coals at meso and macro scales they could be considered as the first approximation, as brittle isotropic solids. Here we discuss models of indentation of materials that due to action of the indenters, change their structure within the specific regions. The crushed regions have internal structures that differ from the initial structure of non-damaged materials. If one considers the mechanical behaviour of the initial material that has got these regions then it should be classified as plastic. Indeed, the material that was deformed by an external load, does not restore its original shape after unloading, i.e. there is no elastic potential and the work done by the stresses to deform material depends on the path of deformation. However, one cannot employ the classic theory of plasticity in a direct way. Due to densification of crushed material, the hydrostatic pressure causes plastic deformations in a way similar to one observed in sintering materials.

It is known that coals of different stages of metamorphism differ in their structure (Hirsch 1954). For example, a "liquid" model was proposed for mid-stage metamorphism coals: weakly ordered graphitized structures are connected by amorphous material structures, and the proportion of amorphous material is comparable to the proportion of relatively small graphitized structures. This fits well with the idea of the unbundling structure of coking coals (high coking

coals), which is the reason for their transition to a liquid state when heated at temperatures of 350-400^o C. For low-rank coals, an "open structure" model was proposed, in which amorphous matter is predominant, and graphitized clusters are distributed unevenly, and the connectivity of structural clusters is realized due to the predominance of cross-links, i.e., chemical bonds. At the same time, high-grade coal and anthracites are characterized by an ordered oriented structure with a large proportion of enlarged graphitized clusters with a low proportion of amorphous matter. In this case, the connectedness of structural clusters is due to prevailing non-covalent interactions, such as van der Waals forces. Therefore, the mechanisms of fracture of coals of different stages of metamorphism may be not the same and they depend on the structure of a coal under consideration. As we have noted above, the properties of coals at meso and macro level, including the elastic modulus and the values of the critical stress intensity factor, of course depend on the properties of their constituent macerals, metamorphism, and many other conditions, however, they are determined experimentally.

Consider a brittle structured material as having the initial porosity θ_0 as a brittle half-space. A conical indenter of semi-vertical angle B is vertically pressed by load P into this half-space (see Fig. 1). The porosity of materials may greatly affect their mechanical behaviour (see, e.g. Shtern et al. 1982, Olevsky 1998, Manoylov et al. 2013). Let the volume of pores in a unit volume of the porous material (the porosity) be θ then the volume of the solid (bulk) part is $1-\theta$. If a porous material has the density ρ and the density of the solid phase is ρ_s, then $\rho = \rho_s(1-\theta)$. In coal samples due to presence of pores and defects that are not visible by optical microscopy, stiffness and flexural strength of the strip-shaped samples extracted from the one chunk of coal may vary in an extremely large range (West et al. 2012). Moreover, the macerals have different porosity characteristics, e.g. vitrinite is mainly characterized by microporosity, the inertinite is dominated by meso- and micropores, while liptinite has a large fraction of macropores. The dividing point between macropores and micropores is often taken as an effective pore radius of 10.0 nm (see, e.g. Xie 2015). Because the porosity of different coal macerals differs, speaking about the initial porosity θ_0, we mean the total initial porosity of a particular coal sample that is estimated as a macro characteristics of the sample. Further, the hardness of a coal maceral determined using microindentation differs considerably of hardness values of the same maceral determined using nanoindentation (Kossovich et al. 2019a).

It is known that the Meyer hardness is the ratio of the applied load to the projected area of indentation, while Martens hardness is hardness under test force; we denote as HM the Meyer hardness under applied load, i.e. $HM = P/(\pi a^2)$. Deformations and fracture of coals depend on many parameters. To model the process under consideration one needs to know elastic characteristics: Young's modulus (E) and Poisson's ratio (ν) of the coal. Because fracture and crushing of the coal is modelled one needs to introduce the following characteristics: the values of strength of the porous material under uniaxial compression (Y) and tension (σ_f). To model fracture of a brittle material one needs to know either its HM or its surface energy γ (alternatively its critical stress intensity factor K_{Ic}).

Analysing elastic-plastic indentation Johnson (1985) noted that it is very difficult to calculate the contact stresses due to an elastic-plastic indentation in practice because the shape and size of the elastic-plastic boundary is not known *a priori*. Hence, he considered a simplified model of an elastic-plastic indentation. This model describes the contact surface of the indenter being encased in a semi-spherical 'core' of radius a and a hydrostatic component of stress is acting within the core. Then for $r > a$, i.e. outside the core, he assumed that the

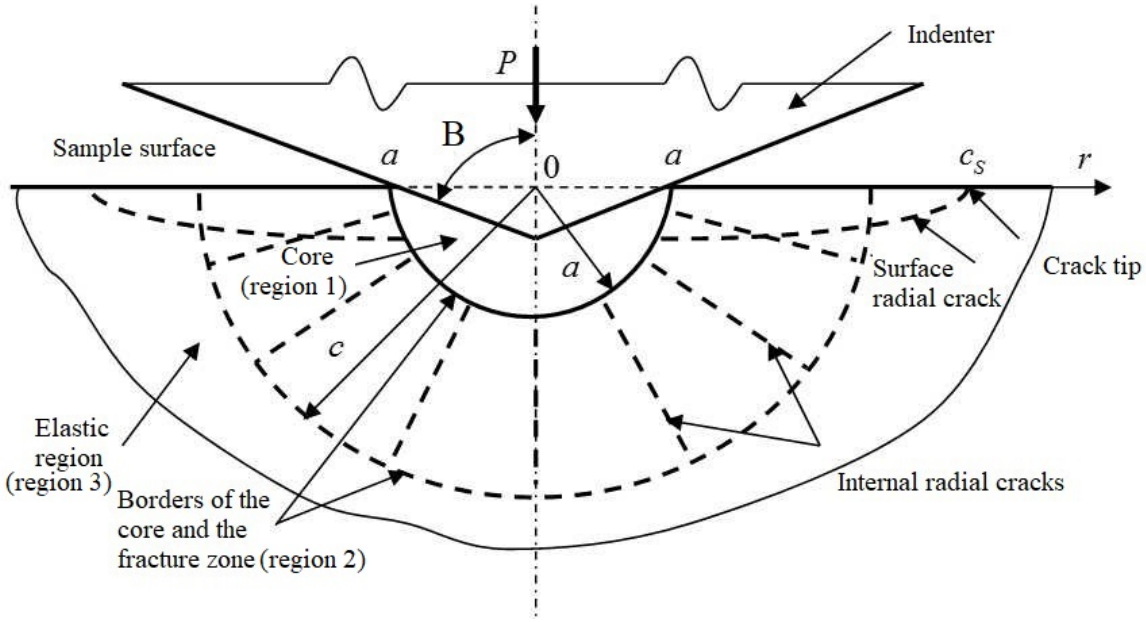

Figure 1: Indentation of a brittle material having a core of crushed particles (the region 1: $0 \leq r < a$), a region of fracture (the region 2: $a \leq r \leq c$), and a region of elastically deformed material (the region 3: $c < r$). Indenter is a cone of semi-vertical angle B. Region 2 contains internal radial cracks along with the surface radial cracks. The size of surface radial cracks c_s exceeds the size of region 2, i.e. $c_s > c$.

stresses and displacements have radial symmetry and are the same as in an infinite elastic, perfectly-plastic body which contains a spherical cavity under a hydrostatic pressure. The Johnson core model was developed further by many authors in particular by Galanov and Grigoriev (2006) and Galanov et al. (2016, 2017).

According to the Galanov-Grigoriev (GG) model (2006), due to action of the indenter, three regions can be delineated (see Fig. 1): (i) an elastic region $r > c$, (ii) an intermediate region $a \leq r \leq c$ having radial crack fracture, and (iii) the core of crushed material $r < a$. Here c is the radius of the fracture region, and a is the radius of the contact area between the indenter and the sample) and this radius is equal to the radius of the semi-spherical core. It is also assumed that the radial displacement $u_r(r)$ is a continuous function of r argument within all regions.

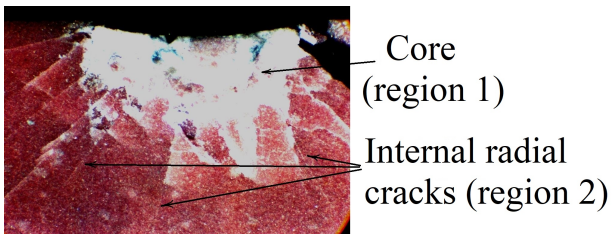

Figure 2: An image of the core and fracture regions within Al_2O_3 ceramic composite (after Grigoriev et al. 2013).

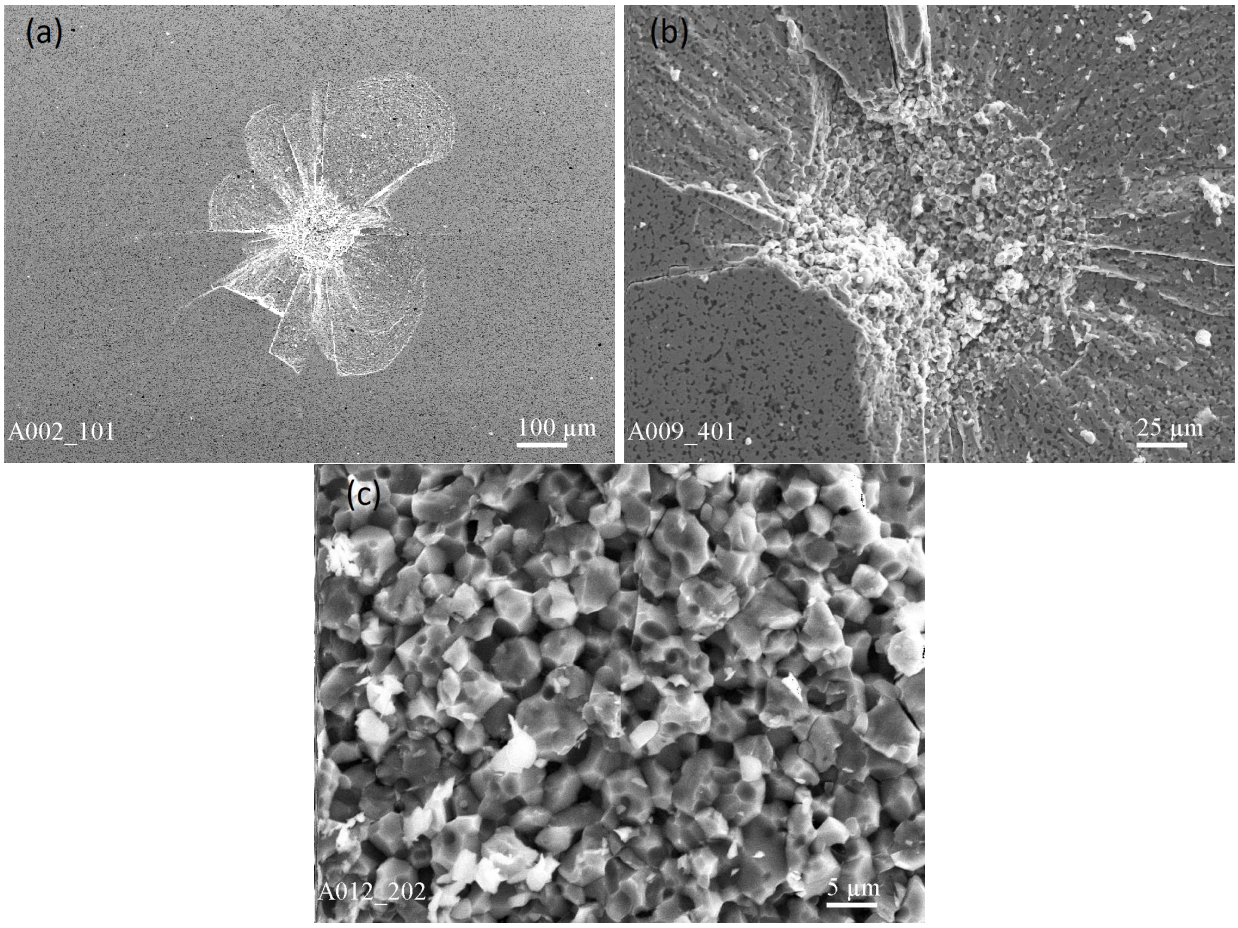

Figure 3: Images of the core and fracture regions within $ZrB_2 - SiC$ ceramic composite (due to O.N. Grigoriev): (a) an imprint with a core region and surface lateral cracks; (b) the core and the surrounding regions uncovered by the lateral cracks; and (c) the granular stricture of the crushed region (the dust particles of the core).

It is difficult to check visually the applicability of the GG model assumptions to coals because normally only very thin coal samples are transparent (see a discussion by Borodich et. al. 2015); the coal structures at atomic/nano level were studied using X-rays (see, e.g. Hirsch 1954). However, this model can be supported by considering the images of fracture within a transparent sample of a ceramic Al_2O_3 sample (see Fig. 2), and where one can observe both the core of crushed material along with radial cracks (Grigoriev et al. 2013). In the processes under consideration, surface radial and lateral cracks are essentially radial volume cracks in the dilation region, however the shapes of the cracks are modified by the presence of a free surface of the sample and the processes of loading and unloading the sample. After unloading the sample, the lateral cracks reveal the deformed and fractured state of the sample in the core and its surroundings, making it available for observation in a plane parallel to the sample surface (see Fig. 3). The cracks start from the surface of the core and have no significant effect on the stress-strain state and fracture of the sample represented by the core model.

3 Modelling of material fracture and crushing.

The indentation problem under consideration is axisymmetric.

3.1 Fracture and crushing regions according to the GG model.

Let us consider the above mentioned regions separately following the ideas by Galanov and Grigoriev (2006). Because there are neither electronic version of the paper nor its translation into English, for the sake of completeness, we present a concise version of the GG model as applied to a new kind of materials.

Volumetric strain within the material is expressed as $e = \sum \partial u_k/\partial x_k$. Note that $e < 0$ for $r < a$ due to irreversible compaction of the material; $e > 0$ (material dilated) for $a \le r \le c$ due to development of radial cracks and pores, and as it is shown below, the volumetric part of the stress tensor is equal to zero for $r > c$ and, therefore, $e = 0$ in this region.

Region 3. The elastic region is located at $c < r$. Here we have the following equations of equilibrium, constitutive relations and expressions for strains in our axisymmetric problem

$$\frac{d\sigma_r}{dr} + 2\frac{\sigma_r - \sigma_\beta}{r} = 0, \tag{1}$$

$$e_r = \frac{1}{E}\left(\sigma_r - 2\nu\sigma_\varphi\right), \quad e_\beta = e_\alpha = \frac{1}{E}\left[(1-\nu)\sigma_\varphi - \nu\sigma_r\right],$$

$$e_r = \frac{du}{dr}, \quad e_\beta = e_\alpha = \frac{du}{dr}$$

where σ_r and σ_β are radial and hoop stresses respectively, ϵ_r is a radial strain, and $\epsilon_\beta = \epsilon_\alpha$ are hoop strains.

The condition at the infinity and boundary conditions are

$$\lim_{r\to\infty} u_r(r) \to 0, \quad \sigma_\alpha(r = c) = \sigma_\beta(r = c) = \sigma_f.$$

Solving the problem, one obtains

$$u_r = \frac{1+\nu}{E}\sigma_f\frac{c^3}{r^2}, \quad \sigma_r = -2\sigma_f\left(\frac{c}{r}\right)^3, \quad \sigma_\beta = \sigma_f\left(\frac{c}{r}\right)^3, \quad r \ge c, \tag{2}$$

and, for the radial displacement $u_r(c)$ we have

$$u_r(c) = \frac{1+\nu}{E}c\sigma_f. \tag{3}$$

It follows from (2) that in the elastic region the hydrostatic pressure $p = -(\sigma_r + 2\sigma_\beta)/3 = 0$, and the volumetric strain $e = e_r + 2e_\beta = 0$.

Region 2. It is located at $a \le r \le c$. This region material is dilated due to radial cracks. It will be shown that the volumetric strain in this region is not constant; in fact, it increases in the opposite direction to r from $e = 0$ at $r = c$, to $e = e_c$ at $r = a + 0$. For such volumetric strain and stress fields, the radial cracks become opened up, i.e. they have some volume, and create pores, however, the model considers the Region 2 as a continuous medium and it does not use any specific description of a pore or a crack that cause the dilation.

At the boundary $r = a$ the stresses in the dilatation region correspond to the following boundary conditions

$$\sigma_r(r = a + 0) = -HM; \quad \sigma_\beta(r = a + 0) = \sigma_\alpha(r = a + 0) = 0. \tag{4}$$

At the boundary $r = c$ the stresses are

$$\sigma_r(r = c - 0) = -2\sigma_f; \quad \sigma_\beta(r = c - 0) = \sigma_\alpha(r = c - 0) = 0. \tag{5}$$

At the boundary $r = c$ the stresses σ_r are continuous, whereas $\sigma_\beta, \sigma_\alpha$ have discontinuity. Hence, the stress-strain state within the Region 2 (the dilatation and fracturing region) is determined by the following equations

$$\frac{d\sigma_r}{dr} + 2\frac{\sigma_r}{r} = 0, \tag{6}$$

$$\sigma_r = E\frac{du_r}{dr}, \tag{7}$$

with boundary conditions (4) for equation (6) and boundary conditions (3) for equation (7).

Integrating (6) and (7), one obtains

$$\sigma_r = -HM\left(\frac{a}{r}\right)^2, \tag{8}$$

$$u_r = \frac{HM}{E}a\left(\frac{a}{r} - \frac{a}{c}\right) + \frac{c\sigma_f(1+\nu)}{E}. \tag{9}$$

From (5), (7) and (9), taking into account the continuity of the radial stresses at $r = c$, the location of the failure front is determined as

$$c = a\sqrt{\frac{HM}{2\sigma_f}}. \tag{10}$$

Let us denote as k the ratio

$$k = a/c = \sqrt{\frac{2\sigma_f}{HM}}. \tag{11}$$

It follows from (10) that the dilatation and fracturing region ($c > a$) exists for materials for which the condition $2\sigma_f < HM$ is satisfied. It is assumed further this condition to be valid. This fact and equality (9) allow us to obtain the following relation at $r = a + 0$ in the considered region:

$$u_r = \frac{HM}{E}a\left(1 - \frac{(1-\nu)}{2}k\right), \tag{12}$$

$$e_r = \frac{du_r}{dr} = -\frac{HM}{E} < 0; \quad e_\beta = \frac{u_r}{a} = \frac{HM}{E}\left(1 - \frac{(1-\nu)}{2}k\right),$$

$$e(a + 0) \equiv e_c = e_r + 2e_\beta = \frac{HM}{E}a\left(1 - (1-\nu)k\right).$$

As the material fracturing leads to pores formation, and the volumetric strain rate de/dt is connected with the porosity change rate $d\theta/dt$ by the differential law

$$de = \frac{d\theta}{1-\theta}, \tag{13}$$

then, the material porosity θ in the dilatation region at $r = a + 0$ that was formed after fracturing, may be determined from the integral equation (13) as

$$e = \ln \frac{1-\theta_0}{1-\theta} \tag{14}$$

where θ_0 is the initial porosity that can be taken at the boundary $r = c$.

Fortunately, in the framework of the present model, the equation (13) may be integrated within the Region 2 without the use of any incremental technique usually employed in theories of deformation of sintered or porous materials. Therefore, we obtain the connection between distributions of stresses and the porosity. It follows from (14) that the 'final' porosity θ^* at $r = a + 0$ is

$$\theta^* = 1 - (1-\theta_0)\exp(-e_c). \tag{15}$$

Hence, the additional porosity of the material due to disintegration and fracturing (the induced porosity) θ_c in the region $a < r < c$ is

$$\theta_c = 1 - \exp(-e_c). \tag{16}$$

Note that in this region, the volumetric strain $e = e_r + 2e_\beta$.

Region 1. The core has radius $r = a$ and it consists of the fully crushed and compressed material, i.e. the material within this region is being crushed by the shear stresses and then packed. The model uses the assumptions similar to ones used by Johnson (1985), i.e. the pressure in the core is close to hydrostatic. The porosity θ_k arises at $r = a - 0$ from fractured material of Region 2 having porosity θ^* by its compaction to θ_k.

The deformations of the crushed medium can be described by the following equations that are based on equations of plasticity of sintered materials (Shtern et al. 1982, Olevsky 1998, Galanov and Grigoriev 2006)

$$\begin{cases} \dfrac{p^2}{\psi} + \dfrac{\tau^2}{\varphi} = \dfrac{2}{3}(1-\theta)\,Y^2, \\ \varphi p = s\psi\tau, \end{cases} \tag{17}$$

where

$$p = \frac{\sigma_1+\sigma_2+\sigma_3}{3}, \quad \tau = \frac{1}{\sqrt{3}}\left[(\sigma_1-\sigma_2)^2 + (\sigma_2-\sigma_3)^2 + (\sigma_1-\sigma_3)^2\right]^{1/2},$$

$\sigma_1, \sigma_2, \sigma_3$ are principal stresses. The following notations (Olevsky 1998) are used $\psi = 2(1-\theta)^3/(3\theta)$ and $\varphi = (1-\theta)^2$ that are functions of porosity θ. The system (17) includes the index of the deformed state s (see, e.g. Shtern et al. 1982) that is determined as the ratio of the rates of volumetric ($\dot{e}$) and shear ($\dot{\Gamma}$) strains $s = \dot{e}/\dot{\Gamma}$. It can be shown that $s = -\sqrt{3/2}$ (see Appendix A). This value of the index corresponds to compression of the porous medium in a spherical mold.

The system of equation (17) is similar to equations of plasticity and therefore, they can be treated as equations of 'quasi-plasticity' of the porous medium. Indeed, if one determines an equations of a yield surface in theory of plasticity, in the GG model the latter equation of the system determines the surface of fracture.

At the front $r = a$, the former equation in (17) could be considered at the condition of crushing of the material by shear stresses. The material porosity in this case is determined by (16), i.e. $\theta = \theta_c$. The latter equation in (17) may be considered as an associated law of crushing and packing of the material in Region 2, having induced porosity $\theta = \theta_c$. Therefore, crushing and packing of the material in Region 2 at the front $r = a$ is considered to be quasi-plasticity of the porous material.

Substituting

$$\theta = \theta_c, \quad p = \frac{\sigma_r + 2\sigma_\beta}{3}, \quad \tau = \sqrt{\frac{2}{3}}\left|\sigma_r - \sigma_\beta\right|, \quad \sigma_r = -HM,$$

into the conditions (17) at the front $r = a$ and excluding σ_β, we obtain the following formulae for HM that is similar to the famous Tabor law (Johnson 1985)

$$HM = CY, \quad C = K\frac{(1-\theta_c)^{3/2}}{\sqrt{\theta_c}}, \quad K = \frac{2\left(\theta_c - \sqrt{2/3}(1-\theta_c)s\right)}{3\sqrt{\theta_c + 2/3(1-\theta_c)s^2}} = \frac{2}{3}, \tag{18}$$

where the 'induced' porosity θ_c is defined by the following relation

$$\theta_c = 1 - \exp(-e_c), \quad e_c = \frac{HM}{E}\left[1 - (1-\nu)k\right] > 0. \tag{19}$$

One can estimate the work spent to fracture of the material. It follows from the GG model (see Appendix B) that the energy spent for crushing all material of the core is

$$A_{3f} = \frac{\pi HM^2 a^3}{3E}\left[1 + \frac{2(1+3\nu)}{HM^2}\sigma_f^2\right] \tag{20}$$

This expression will be used further to estimate the sizes of dust particles.

3.2 Statistical characteristics of dust particles

Crushing of glass samples was studied by Galin, Cherepanov and their co-authors assuming that all particles have the same size. Their approaches may be found in a book by Cherepanov (1979). If we consider dust particles as spherical then we can take the particle radius R as its characteristic size. Note that assumption of equal sizes of all particles (Cherepanov 1979), i.e. the probability distribution function is the Dirac delta function, is a quite rough approximation that may lead to controversial conclusions. Therefore, we assume that the probability density function $p(R)$ of the radii of crushed particles (R) satisfy the uniform distribution

$$p(R) = \begin{cases} R_m^{-1}, & 0 < R \le R_m \\ 0, & R \le 0, R_m < R. \end{cases}$$

The main basis for the assumption of uniform probability density function of particle sizes in the core is the almost homogeneous pressure in the core. Indeed, $p = HM\,(1-\theta_k)$ where θ_k is small (see Appendix B).

It is clear that the mathematical expectation (mean) of the distribution is $m = R_m/2$ where R_m is the maximum size of the particle, while the dispersion $\sigma^2 = R_m^2/12$.

By definition, dust particles include particles whose diameters d are within the following interval $d_0 = 1\mu m \le R \le d_1 = 100\mu$ m. Hence, we have

$$P(d_0 \le d \le d_1) \equiv P(R_0 \le d \le R_1) = \int_{R_0}^{R_1} p(R)dR = \frac{R_1 - R_0}{R_m} = \frac{d_1 - d_0}{2R_m}.$$

The value $P(d_0 \le d \le d_1)$ defines the ability of a coal to create dust particles. This ability may be estimated using the methods of continuous fracture mechanics on the basis of measurements of the hardness HM of coals. Evidently, HM for different coals should be measured applying the same compressive load.

The volume of the core is $(2/3)\pi a^3$, therefore, it follows from (20) that the energy Π spent for crushing a unit volume of the core is

$$\Pi = \frac{A_{3f}}{2\pi a^3} = \frac{HM^2}{2E}\left[1 + \frac{1+3\nu}{2}k^4\right]. \tag{21}$$

On the other hand the size R_m is defined from the energy equation

$$\Pi = 3\gamma \left[\int_0^{R_m} R^2 p(R)dR\right] / \left[\int_0^{R_m} r^3 p(R)dR\right] = \frac{4\gamma}{R_m} \tag{22}$$

for a volume unit of crushed material. Comparing (21) and (22), one obtains the radius of the maximum particle and the mathematical expectation of the particle size respectively

$$R_m = 4\gamma/\Pi, \quad m = 2\gamma/\Pi. \tag{23}$$

The effective fracture surface energy γ of a coal sample can be estimated by its critical stress intensity factor K_{Ic} as

$$\gamma = \frac{1-\nu^2}{2E}K_{Ic}^2.$$

Then (23) can be written as

$$R_m = \frac{2(1-\nu^2)}{E\Pi}K_{Ic}^2, \quad m = \frac{(1-\nu^2)}{E\Pi}K_{Ic}^2. \tag{24}$$

An alternative estimation of γ may be obtained by correlative connection of K_{Ic} and compressive strength of the coal sample σ_c.

Some preliminary studies (Epshtein et al. 2020) showed that the petrographic composition (maceral composition) of coals has a significant effect on their ability to fracture and crushing. Therefore, in order to reduce the uncertainty introduced by petrographic composition on the results of mechanical tests, we used coals with a high content of vitrinite (Table 1). Microhardness on coals was also determined on vitrinite group macerals in accordance with the standard microindentation method described in the state standard (GOST 21206-75).

Naturally coals are characterized not only by their mechanical properties but also by other indicators. Here the following indicators are presented: the mean random vitrinite reflectance index $R_{o,r}$, the vitrinite content Vt , the inertinite content I, the liptinite content L, the total moisture Wt, the ash on dry basis A^d, the volatiles yield on dry ash-free basis V^{daf}, the gross calorific value on dry ash-free basis Q_s^{daf}, the sulphur contents on dry basis S_t^d, and the plastic layer thickness Y_l. Plastic layer thickness is used to characterize the bituminous coals ability for transition from solid to liquid phase during heating at temperatures range of 300-450 ^{o} in non-oxidizing environment. This index is determined using the so-called plastometric curve denoting the bulk alteration of coal in time at a given mode of temperature raise. The larger Y_l, the higher the so-called caking ability of the coal. Table 1 shows the main indicators reflecting the petrographic composition, rank and quality of coals originating from the Kuznetsk coal basin, used as an example of applying the proposed model.

Table 1: Main indicators of coals used in experiments.

Coal Kind	$R_{o,r}$, %	Vt, %	I, %	L, %	Wt, %	A^d %	V^{daf}, %	Q_s^{daf}, MJ/kg	S_t^d	Y_l, mm
I	0.7	88	9	3	6.3	7.5	41.2	32.6	0.6	6
II	0.9	93	7	-	4.1	7.8	38.5	35.8	0.5	31
III	1.8	7 3	27	-	3.9	14.6	13.4	34.9	0.5	0

Three kinds of coals of different stages of metamorphism were tested: (i) a) a bituminous coal having the mean random vitrinite reflectance index $R_{o,r} = 0.7\%$ (kind I); (ii) aa bituminous coal having $R_{o,r} = 0.9\%$ and high caking ability; its plastic layer thickness is $Y_l = 31$ mm (kind II); and (iii) a bituminous coal having $R_{o,r} = 1.8\%$ and $Y_l = 0$ (kind III).

Coals were sampled from coal seams according to standard methods (see GOST 21206-75). According to the standard, pieces of 30-50 mm long were from each kind of coals. As test pieces, polished sections were prepared such that the polished surface is oriented perpendicular to the bedding direction. At least two randomly selected testing surfaces were prepared from each sample of a coal. Microhardness measurements were performed on vitrinite group macerals, in an optically homogeneous region having no cracks and mineral inclusions. From thirty to fifty measurements were made on a single sample at different sections of vitrinite. For specified kind of the coals, the average of the measured microhardness values for all samples was calculated and used in the model if the standard deviation from the average for all measurements did not exceed 5%. After sampling, the samples were placed in sealed containers to exclude the influence of oxidation on the properties of the coals. The coals were chosen according the following principles: (i) they have close petrographic compositions having predominant vitrinite content (the range of vitrinite contents in coals is 73-93%); (ii) they have a significant difference in caking ability characterized by Y_l. One can see from Table 1 that even if the coals of kind I and kind II have small difference in terms of vitrinite reflection index, they differ significantly in terms of caking ability. The coal of kind III has a high vitrinite reflectance and it is characterized by a complete absence of caking ability. Thus, the selected bituminous coals are close in petrographic composition, however, they have different vitrinite reflectance and they differ significantly in terms of caking ability in the series of metamorphism of bituminous coals which indicates the differences in their structure (see, e.g. Hirsch 1954).

Let us consider the above described coals of varying stages of metamorphism. Using their mechanical properties including the average hardness HM of coals, along with the above described GG model, one can estimate the size distribution of the dust particles formed within the region of fully crushed material (Region 1). In Table 2 we present the characteristics of the coals. Some data for Table 2 was taken from the handbook tables presented by Shtumpf et.al. (2014) and the list was extended by the results of our custom experiments described above.

Table 2: Mechanical properties of coals of varying stages of metamorphism.

Coal Kind	E, GPa	ν	Y, MPa	σ_f, MPa	HM, MPa	K_{Ic}, MPa$\cdot$ m$^{3/2}$
I	6	0.23	14.8	1.22	320	0.26
II	10	0.16	20	2.2	260	0.5
III	3	0.26	13.9	1.4	380	0.31

Using the data of Table 2, we can use the equations (11), (21), and 24) in order to estimate the sizes of the dust particles in the bituminous coals of the above described kinds. The results of the calculations are presented in Table 3.

Table 3: Ratio of fracture front's radii k, energy spent for crushing of a unit volume of the core Π, average m and maximum R_m sizes of the coal dust in coals of varying stages of metamorphism.

Coal Kind	k	Π, MJ	m, μm	R_m, μm
I	0.087	8.534	1.25	2.5
II	0.13	3.381	7.2	14.4
III	0.086	24.1	1.24	2.48

One can see that the sizes of dust particles of bituminous coals of low and high stages of metamorphism are practically the same, while the dust particles of the middle stage of metamorphism are almost six-times larger than in the coals of other stages. Note that although quantitatively, the radii of the crushed material particles for coals of low and high stages of metamorphism are comparable, this does not mean that the fracture mechanism are the same. In fact, these mechanisms should differ from each other and they depend on the structure of the studied coals and properties of constituent macerals. However, as it has been explained above, the present model works with average macroscale fracture characteristics. The modern methods of measurment of hardness are based on the use of depth-sensing indentation (DSI) techniques (see, a review by Borodich 2014). These analytical treatments of the DSI experiments are usually based on the Oliver-Pharr approach (see, e.g. Oliver and Pharr 1992, Fischer-Cripps 2011). If one applies an alternative approach introduced by Galanov and Dub (2017) then one can show (Kossovich et al. 2019a) that the values of HM are lower than the values obtained by Oliver-Pharr approach. One can see from (21) and (22) that, if HM increases, then the values of R_m will decrease in turn.

4 Discussion and Conclusion

Fracture, crushing and dust formation of bituminous coals under action of hard tools are problem of great practical importance for the mining industry. Currently there are not theoretical models describing these complex phenomena. Here for the first time, the problems of crushing and dust formation of coals are studied using the Galanov-Grigoriev model.

It follows from the classic Griffith idea that fracture of elastic brittle solids is connected to the amount of energy released due to fracture. To calculate this energy in brittle coals, one needs to consider the stress fields in all regions separated by the fronts $r = c$ and $r = a$. Fracture at the front $r = c$ and development of cracks in Region 2 induce additional porosity of the material (coal). Then, in Region 1 (the core), one observes crushing of this fractured material and its compaction. According to the GG model the material behaviour in the core is described by the system(17) that is an analogy to models of plasticity of porous or sintered materials (see, e.g. (5.1)-(5.3) by Shtern et al. 1982) that actually neglect the elastic strains and the solid phase is considered as incompressible material. Therefore, there is some contradiction in the model assumptions, namely we estimate the energy spent for crushing a unit volume of the core, while, on the other hand, the elastic strains are neglected by the system(17). To compensate the neglect of the elastic strains and in turn, to overcome the contradiction, the elastic energy released in the core (the region of fully crushed material) is calculated as a sum of the jumps of work of elastic deformations at the fronts $r = c$ and $r = a$ (see Appendix B).

As we have noted above, there is an analogy in modelling of fracture of coals and polycrystalline metals. If properties of individual crystals of a steel sample are different, each crystal is anisotropic and has its own orientation in space. However, to model cracking of a metal sample, one considers the sample as an isotropic solid with an average value of the critical stress intensity factor K_{Ic}. The K_{Ic} values are determined experimentally. In coals, a similar situation is observed. At the nano and micrometre level, they consist of various macerals and they have a layered structure, however, at this stage, we model the coals as a brittle isotropic material. The properties of this material, including the elastic modulus and the values of the critical stress intensity factor, of course depend on the properties of their constituent macerals, metamorphism, and many other conditions, however, they are determined experimentally from macroscale experiments. Studying porous materials, one can get the macro-hardness of the material HM experimentally by indentation of the material by a relatively large load when the hardness gets stable values that are not affected by bluntness of the indenter. Other parameters of the problem: E, ν, σ_f, K_{Ic} and θ_0 are also measured experimentally. Then applying the Galanov and Grigoriev (2006) model one can analyse the core of fully crushed material in detail. For example, using the system of non-linear equations (18) and (19), one can calculate the compressive strength of the material Y

$$Y = \frac{3\sqrt{\theta_c}}{2\left(1-\theta_c\right)^{3/2}} HM.$$

Note that the relation Y as a function of HM is non-linear because θ_c is also a function of HM. The model can be also applied to calculate the density of the material within crushed Region 1.

As it has been mentioned above, here the GG model was applied to the problem of crushing of porous brittle solids and dust formation under instrumented indentation. The results obtained are important in predicting the yield of airborne respirable dust with particles whose sizes are less than 10 microns (the amount of such particles is used for determination of the degree of atmospheric air pollution). Particles of such sizes may remain in air as suspended dust for a long time. Although our approach is valid in application to many other porous brittle materials, we concentrated on bituminous coal particles as an important source of environmental contamination. The energy spent for crushing of a unit volume of the core Π was calculated and used to estimate the average m and the maximum R_m sizes of the coal dust in coals of varying stages of metamorphism. Our results show that in all cases there are no particles that are greater than the upper limit for crushed dust particles, however there are nanodust particles.

5 Acknowledgment

The work was supported by Russian Science Foundation grant (project No. 18-77-10052).

The authors are grateful to Professor O.N. Grigoriev (Institute for Problems in Materials Science, National Academy of Sciences of Ukraine) for providing them by images of fracture of ceramics used in this paper.

Thanks are due to reviewers of the paper for their valuable comments to the content of the paper.

Appendix A.

The index of the deformed state s.

It is known (Shtern et al. 1982) that the rate ($\dot{\Gamma}$) of second deviatoric stress invariant (Γ)

$$\Gamma = \frac{1}{\sqrt{3}}\sqrt{(\epsilon_1-\epsilon_2)^2+(\epsilon_1-\epsilon_3)^2+(\epsilon_2-\epsilon_3)^2}$$

may be used as a scalar characteristic of material deformation at constant volume. Here ϵ_1, ϵ_2, and ϵ_3 are the principal strains. For our spherically symmetric problem, we have $\epsilon_1 = \epsilon_r$, $\epsilon_2 = \epsilon_3 = \epsilon_\beta$. Hence, we have

$$\Gamma = \sqrt{\frac{2}{3}}|\epsilon_r - \epsilon_\beta| = \sqrt{\frac{2}{3}}\frac{< p >}{E}\left(2 - \frac{(1-\nu)}{2}\sqrt{\frac{2\sigma_f}{< p >}}\right). \tag{A1}$$

Let us calculate the index of the deformed state s at the front $r = a$. By definition we have

$$s = \frac{\dot{e}}{\dot{\Gamma}} = \frac{de}{d\Gamma} = \frac{e^+ - e^-}{\Gamma^+ - \Gamma^-} \tag{A2}$$

where the signs $'+'$ and $'-'$ denote the values of the functions before (at $r = a + 0$) and after the front (at $r = a - 0$), respectively.

By substitution of (A1) into (A2), we get

$$s = \sqrt{\frac{3}{2}} \frac{e^+ - e^-}{|\epsilon_r^+ - \epsilon_\beta^+| - |\epsilon_r^- - \epsilon_\beta^-|}. \tag{A3}$$

Taking into account that $e_r < 0$ and $e_\beta > 0$, while $\epsilon_\beta^+ = \epsilon_\beta^-$, we obtain from (A3) the value we have declared above

$$s = \sqrt{\frac{3}{2}} \frac{e^+ - e^-}{-\epsilon_r^+ - \epsilon_\beta^+ + \epsilon_r^- - \epsilon_\beta^-} = \sqrt{\frac{3}{2}} \frac{e^+ - e^-}{-\epsilon_r^+ + \epsilon_r^-} = \sqrt{\frac{3}{2}} \frac{e^+ - e^-}{-e^+ + e^-} = -\sqrt{\frac{3}{2}}.$$

Appendix B.

Works of elastic deformations and material crushing.

In the spherical system of coordinates, the specific work of elastic deformation per volume unit could be written in the following form

$$w_e(r) = \frac{1}{2E} \left[\sigma_r^2 + 2\sigma_\beta^2 - 2\nu(\sigma_\beta^2 + 2\sigma_r\sigma_\beta) \right]. \tag{B1}$$

For the region 3, substituting equation expressions (2) into (B1) we get

$$w_e(r) = \frac{3\sigma_f^2(1+\nu)}{E} \left(\frac{c}{r}\right)^6, \tag{B2}$$

and the elastic energy stored in Rregion 3 $r \geq c$ equals to

$$A_1 = \iiint_{r \geq c} w_e dV = \frac{2\pi(1+\nu)\sigma_f^2}{E} c^3 = \frac{\pi(1+\nu)kHM^2}{2E} a^3. \tag{B3}$$

Substituting $r = c$ into (B2), one can estimate the energy of elastic deformation A_2 stored in the region $r \leq c$ before its crushing

$$A_2 = \frac{2}{3}\pi c^3 w_e = \frac{2\pi(1+\nu)\sigma_f^2}{E} c^3. \tag{B4}$$

For the region 2, one can get from (B1)

$$w_e = \frac{HM^2}{2E} \left(\frac{a}{r}\right)^4. \tag{B5}$$

and the stored elastic energy A_3 in this region

$$A_3 = \iiint_{a \leq r \leq c} w_e dV = \frac{\pi HM^2}{E} a^3 (1-k). \tag{B6}$$

Substituting $r = a$ into (B5), one can estimate the energy of elastic deformation A_4 stored in the region $r \leq a$ before its crushing and formation of the fragmented core material

$$A_4 = \frac{2}{3}\pi a^3 w_e = \frac{\pi HM^2}{3E} a^3. \tag{B7}$$

This part of elastic energy is released at the front $r = a$ and causes to transformation of coal to the powder of the core. It will be shown below that this part of energy is the main part of energy spent for the core formation.

Galanov and Grigoriev (2006) calculated the average porosity of the core θ_k, the volumetric strain of the solid phase (e_{ks}) after it has been compressed by the hydrostatic pressure $p_s = p/(1-\theta_k)$, and the average volumetric strain e_k in the core taking into account the volume of the indenter part penetrated into the material. In particular, they derived the following formulae

$$\theta_k = \sup\left\{1 - \frac{(1+e_{ks})(1-\theta^*)}{1+e_k},\, 0\right\}, \quad e_{ks} = -\frac{3HM(1-2\nu)}{E}$$

and

$$e_k = -\frac{\cot \mathrm{B}}{2} + \frac{3}{2}\frac{HM}{E}\left[2-(1-\nu)k\right] + \frac{8(1-\nu_i^2)HM}{\pi E_i}$$

where E_i and ν_i are the elastic modulus and Poisson's ratio of the indenter.

After the formation of the fragmented core, the core can be considered as an elastic material having porosity θ_k and subjected to the hydrostatic pressure $p = -HM(1-\theta_k)$.

The specific elastic energy stored per volume unit is

$$w_e = \frac{p^2}{2K_{ef}} = \frac{HM^2(1-\theta_k)^2}{2K_{ef}}, \quad K_{ef} = \frac{E}{3(1-2\nu)}(1-\theta_k) \tag{B8}$$

where K_{ef} is an effective elastic bulk modulus of porous material for small values of θ_k. Then the elastic energy A_4 stored in the core is

$$A_5 = \frac{HM^2(1-2\nu)}{E}(1-\theta_k)\pi a^3. \tag{B9}$$

Using (B3), (B4), (B6), (B7) and (B9), one can calculate the total work A_e of the elastic deformation during indentation

$$A_e = \sum_{i=1}^{5} A_i = \frac{4\pi(1+\nu)\sigma_f^2}{E}c^3 + \frac{\pi HM^2}{E}a^3\left(\frac{4}{3}-k\right) + \frac{HM^2(1-2\nu)}{E}(1-\theta_k)\pi a^3.$$

That can be written as

$$A_e = \frac{\pi HM^2}{E}a^3\left[\frac{4}{3} + \nu k + (1-2\nu)(1-\theta_k)\right].$$

Note that both the energies released at the front $r = a$ and at the front $r = c$ contribute to the core formation. The latter contribution compensates the neglect of the elastic strains in the system(17). Hence, the elastic energy released in the core is calculated as a sum of the jumps of work of elastic deformations at the fronts $r = c$ and $r = a$. This sum is equal to the energy released due to fracture.

For $r = c$, one has $w_e^+ = \dfrac{3(1+\nu)\sigma_f^2}{E}$, and $w_e^- = \dfrac{2\sigma_f^2}{E}$, then $[w_e](c) = \dfrac{(1+3\nu)\sigma_f^2}{E}$.

Using (B1), one can determine the jump $[w_e](a) = w_e^+ - w_e^-$ of the function w_e at the transition through the crushing front $r = a$. It is assumed that after the crushing $w_e^- = 0$.

Because it follows from (B5) at $r = a$ that $w_e^+ = \dfrac{HM^2}{2E}$, we obtain $[w_e](a) = \dfrac{HM^2}{2E}$. Thus, one has

$$[w_e] = [w_e](a) + [w_e](c) = \frac{HM^2}{2E}\left[1 + \frac{2(1+3\nu)\sigma_f^2}{HM^2}\right].$$

Note that $[w_e](c)$ is small in comparison with $[w_e](a)$.

Finally, the elastic energy released in Region 1 ($r < a$) is

$$A_{3f} = \frac{2}{3}\pi a^3\left(\frac{HM^2}{2E} + \frac{(1+3\nu)\sigma_f^2}{E}\right) = \frac{\pi HM^2}{3E}a^3\left[1 + \frac{2(1+3\nu)\sigma_f^2}{HM^2}\right].$$

This is exactly the expression (20) used for estimation of the sizes of dust particles and it is almost the same as the expression for A_4 in (B7).

References

[1] Argatov, I.I., Borodich, F.M., Epshtein, S.A. and Kossovich, E.L. (2017) Understanding of material properties of thin films attached to substrates: Depth-sensing unloading of elasto-plastic and elasto-brittle materials. *Mechanics of Materials*, **114**, 172-179.

[2] Bernhardt, E.O. (1941) Über die Mikrohärte der Feststoffe im Grenzbereich des Kick'schen Ähnlichkeitssatzes. *Zeitschrift für Metallkunde*, **33**, 135–139.

[3] Borodich, F.M. (2014) The Hertz-Type and Adhesive Contact Problems for Depth-Sensing Indentation. *Advances in Applied Mechanics*, **47**, 225-366.

[4] Borodich, F.M., Bull, S.J. and Epshtein, S.A., (2015) Nanoindentation in studying mechanical properties of heterogeneous materials. *J. Mining Sci.*, **51**, 470–476.

[5] Cherepanov, G.P. (1979) *Mechanics of Brittle Fracture*. McGraw-Hill, New York.

[6] Constantinides, G., Ulm, F.-J. and Van Vliet, K. (2003) On the use of nanoindentation for cementitious materials. *Mat Struct.*, **36**, 191-196.

[7] Epshtein, S.A. Barabanova, O.V., Minaev, V.I., Weber, J. and Shirochin, D.L. (2007) Effect of dimethylformamide treatment of coals on their thermal degradation and elastic-plastic properties. *Solid Fuel Chemistry*, **41**, 210–215.

[8] Epshtein, S.A., Borodich, F.M., Bull, S.J., (2015) Evaluation of elastic modulus and hardness of highly inhomogeneous materials by nanoindentation. *Appl. Phys. A Mater. Sci. Process*, **119**, 325–335.

[9] Epshtein, S.A., Kossovich, E.L., Vishnevskaya, E.P., Agarkov, K.V., Koliukh, A.V. (2020) Determination of total and fine airborne dust in coals. *Min. Informational Anal. Bull.*, No 6., 5-14. DOI:10.25018/0236-1493-2020-6-0-5-14

[10] Fischer-Cripps, A.C. (2011) *Nanoindentation*. Springer.

[11] Galanov, B.A. and Dub, S.N. (2017) Critical comments to the Oliver-Pharr measurement technique of hardness and elastic modulus by instrumented indentations and refinement of its basic relations. *J Superhard Mater*, **39**, 373-389. doi: 10.3103/S1063457617060016

[12] Galanov, B.A. and Grigoriev, O.N. (2006) Analytical model of indentation of brittle materials. In: "Electron Microscopy and Materials Strength", Eds.: S.A. Firstov et al. *Proceedings of Institute of Materials Science, Vol. 13*, Kiev, 4-42. (Russian)

[13] Galanov, B.A., Milman, Yu.V., Chugunova, S.I., Goncharova, I.V. and Voskoboinik, I.V. (2017) Application of the improved inclusion core model of the indentation process for the determination of mechanical properties of materials. *Crystals 2017*, **7**, 87; doi:10.3390/cryst7030087

[14] Galanov, B.A., Milman, Yu.V., Ivakhnenko, S.A., Suprun, O.M., Chugunova, S.I., Golubenko, A.A., Tkach, V.N., Litvin, P.M. and Voskoboinik, I.V. (2016) Improved inclusion core model and its application for measuring the hardness of diamond. *J. Superhard Mater.*, **38**, 289-305.

[15] Grigoriev, O.N., Galanov, B.A., Ivanov, S.M. and Kotenko, V.A. (2013) Impact-resistant ceramics. In: *"Physical-Technical Problems of Modern Materials Science", Eds.: I.K. Pokhodnya et al., Vol. 1*, Academic Periodics, Kiev, 390-424. (Russian)

[16] GOST 21206-75 (1977) *Hard coals and anthracite. Determination method for microhardness and microbrittleness.* (Russian)

that is valid in Russia, Ukraine and many other countries of the former Soviet Union.

[17] Grigorovich, V.K. (1976) *Hardness and Microhardness of Metals.* Nauka, Moscow. (Russian)

[18] Hirsch P.B. (1954) X-Ray scattering from coals. *Proc. R. Soc. A Math. Phys. Eng. Sci.*, **226**(1165), 143-169.

[19] Hower, J., Trinkle, E.J., Raione, R.P. (2008) Vickers microhardness of telovitrinite and pseidovitrinite from high volatile bituminous Kentucky coals. *Int. J. Coal Geology*, **75**, 76–80.

[20] Johnson, K.L., 1985. *Contact Mechanics.* Cambridge, Cambridge Univ. Press.

[21] Kolesnikov, Yu.V. and Morozov, E.M. (1989) *Mechanics of Contact Fracture.* Nauka, Moscow. (Russian)

[22] Kožušníková, A. (2009) Determination of microhardness and elastic modulus of coal components by using indentation method. *Geolines*, **22**, 40-43.

[23] Kossovich, E.L., Borodich, F.M., Bull, S.J. and Epshtein, S.A. (2016) Substrate effects and evaluation of elastic moduli of components of inhomogeneous films by nanoindentation. *Thin Solid Films*, **619**, 112–119.

[24] Kossovich, E.L., Borodich, F.M., Epshtein, S.A., Galanov, B.A., Minin, M.G. and Prosina, V.A. (2019a) Mechanical, structural and scaling properties of coals: depth sensing indentation studies. *Applied Physics A: Materials Science and Processing*, **125**, 195.

[25] Kossovich, E.L., Epshtein, S.A., Borodich, F.M., Dobryakova, N.N. and Prosina, V.A. (2019b) Connections between micro/nano scale heterogeneity of mechanical properties of coals and their propensity to outbursts and crushing. *Mining Informational and Analytical Bulletin*, **5**, 156-172. (DOI: 10.25018/0236-1493-2019-05-0-156-172)

[26] Lawn B.R. (1993) *Fracture of Brittle Solids.* Cambridge University Press, Cambridge.

[27] Manoylov, A.V., Borodich, F.M. and Evans, H.P. (2013) Modelling of elastic properties of sintered porous materials. *Proc. R. Soc. A.*, **469** 2154, Article Number: 20120689.

[28] Meyers, R. (Ed.) (1982) *Coal Structure.* Academic Press.

[29] Musyal, S.A. (1963) Microhardness and microbrittleness as possible parameters for classification of fossil coals. In: *Petrographic Specific and Properties of Coals. Ed. Ammosov, I.I., Ch. 3, 164–188*, Moscow, USSR Academy of Sciences Publisher. (Russian)

[30] Neavel, R.C. (1981) Coal structure and coal science: Overview and recommendations. In: *Coal Structure. Eds.: M.L. Gorbaty, K. Ouchi*, Washington, D.C., ACS

[31] Olevsky, E.A. (1998) Theory of sintering: from discrete to continuum. *Materials Science and Engineering: R: Reports*, **R23**, 41-100.

[32] Oliver, W.C. and Pharr, G.M. (1992) An improved technique for determining hardness and elastic modulus using load and displacement sensing indentation experiments. *J. Mater. Res.*, **7**, 1564-1583.

[33] Shtern, M.B., Serdyuk, G.G., Maksimenko, L.A., Trukhan, Yu.V. and Shulyakov, Yu.M. (1982) *Phenomenological Theories of of Pressing of Powders.* Kiev, Naukova Dumka. (Russian)

[34] Shtumpf, G.G., Ryzhkov, Yu.A., Shalamanov, V.A. and Petrov, A.I. (2014) *Physical and Engineering properties of rocks and coals of Kuznetsk coal basin.* Nedra, Moscow. 447 p. (Russian)

[35] Vranjes, S., Misch, D., Schöberl, T., Kiener, D., Gross, D. and Sachsenhofer, R.F. (2018) Nanoindentation study of macerals in coals from the Ukrainian Donets Basin. *Adv. Geosci.*, **45**, 7383.

[36] West, R.D., Markevicius, G., Malhotra, V.M. and Hofer, S. (2012) Variations in the mechanical behavior of Illinois bituminous coals. *Fuel*, **98**, 213-217.

[37] Xie, K-C., (2015) *Structure and Reactivity of Coal. A Survey of Selected Chinese Coals.* Springer. Heidelberg.